CHEMICAL ENGINEERING TRANSACTIONS
VOL. 120, 2025
A publication of AIDIC
The Italian Association of Chemical Engineering
Online at www.cetjournal.it
Guest Editors: Bing Shen How, Viknesh Andiappan, Denny K.S. Ng, Hon Loong Lam, Petar S. Varbanov

ISBN 979-12-81206-21-2; **ISSN** 2283-9216
DOI: 10.3303/CET25120045

Phase Transition Dynamics of Phase Change Material in the Grille-Capsule Packed Channel

Haonan Jia, Yuhang Tian, Jian Yang*, Qiuwang Wang

MOE Key Laboratory of Thermo-Fluid Science and Engineering, School of Energy and Power Engineering, Xi'an Jiaotong University, Xi'an 710049, China
yangjian81@mail.xjtu.edu.cn

Phase change thermal energy storage technology, with its high energy storage density and near-isothermal heat release characteristics, serves as an effective solution to address the intermittency and fluctuation issues in solar energy utilization, thereby significantly enhancing the stability and utilization efficiency of solar energy systems. The encapsulation of phase change material (PCM) within spherical capsules not only significantly enhances the specific heat transfer area but also effectively addresses the long-standing issues of leakage and corrosion during phase transition processes. Notably, the employment of a grid structure enables rapid and ordered layering of PCM capsules, which not only reduces the flow drag but also creates stable flow channels that enhance heat transfer performance. This study presents a numerical investigation on the phase-change process of PCM within grille-capsule packed channels, focusing on the effects of channel-to-particle diameter ratio (N). The results indicate that, under the same inlet Reynolds number (Re), the melting rate of the PCM inside the spherical capsules decreases as the N increases, while the synchronization of the melting process in spherical capsules at different positions improves. Compared to the channel with N = 1, the complete melting time of PCM at different positions increases by an average of 14.32 %, 31.26 % and 28.7 % for N=1.15, 1.3, and 1.47, respectively, which indicates that the N exerts a significant influence on the thermal transport characteristics.

1. Introduction

Against the backdrop of the accelerated transformation of the global energy structure, the BP Energy Outlook 2024 highlights that investments in low-carbon energy, primarily driven by renewables, have surged by approximately 50 % since 2019. However, despite the rapid growth of low-carbon energy, the increase in its total energy consumption remains insufficient to meet the continuous expansion of global energy demand, leading to a persistent rise in fossil fuel usage. To address this challenge, it is imperative to further accelerate the development of renewable energy. Solar energy, characterized by its abundant resources, mature technology, and continuously declining costs, stands as a pivotal force in driving the global energy transition.

Energy storage systems are critical technologies for addressing the temporal and intermittent issues in solar energy utilization, yet each storage technology possesses its unique advantages and limitations, necessitating optimized selection based on specific application scenarios and requirements (Alva et al., 2024). Among these, spherical capsule-packed thermal energy storage (SPTES) systems with encapsulated phase change materials have garnered significant attention in both scientific research and industrial applications due to their high charging and discharging rates, simple structure, stable thermal efficiency, and modular design, making them one of the most promising systems in efficient thermal energy storage technologies (He et al., 2022). Currently, scholars worldwide have conducted extensive and in-depth research on SPTES systems from multiple dimensions, including system construction, heat transfer enhancement, optimization design, and performance evaluation.

Mao and Zhang (2020) conducted numerical simulations and found that reducing the particle size enhances both energy storage capacity and utilization efficiency, although the shape of the storage tank has no significant impact on energy storage capacity at a fixed volume. Wang et al. (2022) established a medium-high temperature packed-bed latent heat storage (PBLHS) experimental system, demonstrating that the inlet temperature and

Paper Received: 12 May 2025; Revised: 18 August 2025; Accepted: 10 September 2025
Please cite this article as: Jia H., Tian Y., Yang J., Wang Q., 2025, Phase Transition Dynamics of Phase Change Material in the Grille-Capsule Packed Channel, Chemical Engineering Transactions, 120, 265-270 DOI:10.3303/CET25120045

velocity of the heat transfer fluid significantly influence the pressure loss in the PBLHS system. Mao and Cao (2023) employed a one-dimensional non-equilibrium model to investigate the effects of Reynolds number, Stefan number, and spherical capsule diameter on the PBLHS system under three different heat transfer fluids, emphasizing that selecting an appropriate heat transfer fluid is crucial for optimizing thermal storage performance. Hu et al. (2022) utilized a continuous solid-phase model and orthogonal design optimization method to evaluate the total heat storage capacity, heat release capacity, average charging and discharging power, and other thermal characteristics of a coupled packed bed thermal energy storage (PBTES) system, ultimately proposing an optimal configuration. Guo et al. (2023) employed a one-dimensional concentric dispersion model to analyse the differences between cascaded and non-cascaded systems using three distinct PCMs, revealing that the cascaded system exhibits a significantly faster heat transfer rate. Building on experimental investigations into the effects of PCM melting temperature, spherical capsule diameter, and packing volume ratio, He et al. (2024) further optimized the stratified structure by applying the concentric dispersion model.

In addition to optimizing the design of packed systems, many scholars have also conducted in-depth research on improving and optimizing the thermal storage unit (spherical phase change capsules). Some researchers have significantly enhanced the heat transfer efficiency and energy storage performance during the phase change process by incorporating flat fins (Sharma et al., 2022), bionic fins (Hu et al., 2023), nanoparticles (Ghojavand et al., 2022), and expanded graphite (Li et al., 2022) within the spherical capsules. Others have optimized the convective heat transfer process between the heat transfer fluid and the capsules, as well as improved the internal phase change performance, by altering the geometric shapes of the spherical capsules, such as adopting unconventional structures like red blood cell shapes (Chen and Zhai, 2017), gourd shapes (Wang et al., 2022), elliptical shapes (Dong et al., 2022), and golf ball shapes (Jia et al., 2024a). Furthermore, Athawale et al. (2022) employed numerical methods to compare the differences in thermal storage processes between structured and unstructured packed configurations, revealing that the packing arrangement of spherical capsules significantly influences the convective heat transfer process between the heat transfer fluid and the capsules, thereby affecting the overall thermal storage performance. Wang et al. (2018) proposed a grille-sphere composite structured packed bed, providing an efficient and convenient method for achieving structured packing. This structure can be viewed as a combination of multiple sub-channels, each exhibiting similar flow and heat transfer characteristics. Building on this, Yu et al. (2020) investigated the thermal storage performance of spherical capsules within sub-channels at a channel-to-particle diameter ratio of 1, analyzing the effects of the inlet temperature and velocity of the heat transfer fluid. However, to simplify numerical calculations, the natural convection process of the liquid PCM inside the spherical capsules was neglected in this study. In summary, research on grid-packed spherical capsule thermal energy storage systems remains limited, particularly regarding the impact of channel-to-particle diameter ratios on thermal storage performance.

In summary, this study employs numerical methods to investigate the thermal storage performance within packed sub-channels at channel-to-particle diameter ratios of 1, 1.15, 1.3, and 1.47, systematically comparing and analyzing the effects of different N values on the melting process of PCM inside spherical capsules. The selection of N=1 is based on its representation of a tightly packed configuration under extreme conditions; N=1.15 is chosen because the spherical capsules within this structure exhibit only slight misalignment; N = 1.47 is selected due to its maximum porosity; N=1.3 is included to avoid an abrupt transition from N = 1.15 to N = 1.47.

2. Physical model

The physical model of the spherical capsule-packed channel used in the numerical simulation is illustrated in Figure 1. A velocity inlet condition is applied, with air as the working fluid. Inlet and outlet sections are included to ensure uniform inlet velocity and to avoid the influence of backflow at the outlet on the numerical calculations. The surrounding walls of the channel are set as no-slip adiabatic boundaries, while the walls of the spherical capsules are defined as no-slip conditions. The capsules are filled with phase change material RT27, whose thermophysical properties remained consistent with those in previous studies (Jia et al., 2024a).

The channel-to-particle diameter ratio is adjusted by varying the side length (W) of the square cross-section. The Discrete Element Method (DEM) is employed to simulate the process of spherical capsules falling into the container, obtaining the coordinates of each capsule when their velocity approached zero. These coordinates were then used to create a three-dimensional model using the Solidworks software. During the modeling process, efforts are made to maintain consistent packed section lengths for different channel-to-particle diameter ratios. The resulting schematic diagrams of the packed structures are shown in Figure 2. It can be observed that the centers of the capsules in different layers coincide, indicating that the spherical capsules tend to arrange in an ordered manner under the influence of the grid. The geometric parameters of the different packed structures are listed in Table 1.

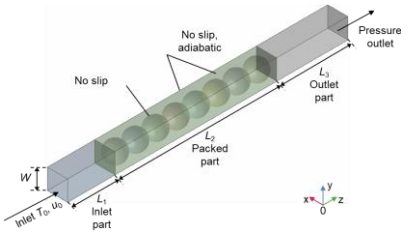

Figure 1: Schematic diagram of the computational domain

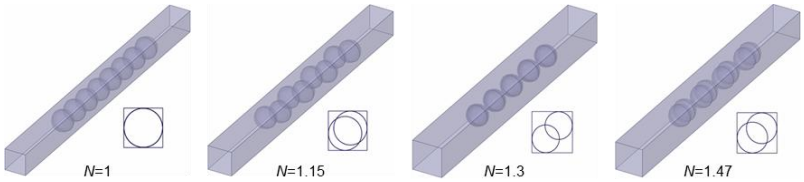

Figure 2: Schematic diagram of the packed structures at different channel-to-particle diameter ratios

Table 1: Geometric parameters of the computational model

N	D (mm)	W (mm)	L_1 (mm)	L_2 (mm)	L_3 (mm)	ε
1	42.6	42.6	100	340.8	150	0.48
1.15	42.6	48.99	100	332.99	150	0.59
1.3	42.6	55.38	100	311.76	150	0.66
1.47	42.6	62.622	100	328.17	150	0.69

3. Numerical methods and model validation

3.1 Numerical equations

This study employs the three-dimensional Navier-Stokes equations to solve the convective heat transfer process between the heat transfer fluid and the spherical capsules. Given the *Re* of 3,000 used in the research, the SST *k-ω* turbulence model is adopted for the calculations, and the governing equations are as follows:

$$\begin{cases} \dfrac{\partial u_i}{\partial x_i} = 0 \\ \rho\left(\dfrac{\partial u_i}{\partial t} + \dfrac{\partial u_i u_j}{\partial x_j}\right) = -\dfrac{\partial p}{\partial x_i} + \dfrac{\partial}{\partial x_j}\left[(\mu + \mu_t)\left(\dfrac{\partial u_i}{\partial x_j} + \dfrac{\partial u_j}{\partial x_i}\right)\right] \\ \rho\left(\dfrac{\partial T}{\partial t} + \dfrac{\partial u_i T}{\partial x_i}\right) = \dfrac{\partial}{\partial x_j}\left[\left(\dfrac{\lambda}{c_p} + \dfrac{\mu_t}{\sigma_T}\right)\dfrac{\partial T}{\partial x_j}\right] \end{cases} \tag{1}$$

$$\begin{cases} \rho\dfrac{\partial k}{\partial t} + \rho\dfrac{\partial k u_i}{\partial t} = \dfrac{\partial}{\partial x_j}\left[\left(\mu + \dfrac{\mu_t}{\sigma_k}\right)\dfrac{\partial k}{\partial x_j}\right] + \tilde{G}_k - Y_k \\ \rho\dfrac{\partial \omega}{\partial t} + \rho\dfrac{\partial \omega u_i}{\partial t} = \dfrac{\partial}{\partial x_j}\left[\left(\mu + \dfrac{\mu_t}{\sigma_\omega}\right)\dfrac{\partial \omega}{\partial x_j}\right] + G_\omega - Y_\omega + D_\omega \end{cases} \tag{2}$$

$$\begin{cases} G_k = \mu_t S^2 \\ \tilde{G}_k = \min\left(G_k, 10\rho\beta^* k\omega\right) \\ G_\omega = \alpha / v_t \tilde{G}_k \end{cases} \tag{3}$$

$$\begin{cases} Y_k = \rho\beta^* k\omega \\ Y_\omega = \rho\beta\omega^2 \end{cases} \tag{4}$$

$$D_\omega = 2\left(1 - F_1\right)\rho\sigma_{\omega,2}\frac{1}{\omega}\frac{\partial k}{\partial x_j}\frac{\partial \omega}{\partial x_j} \tag{5}$$

$$\begin{cases} \sigma_{\mathrm{k}} = \dfrac{1}{F_1/\sigma_{\mathrm{k},1} + (1-F_1)/\sigma_{\mathrm{k},2}} \\ \sigma_{\omega} = \dfrac{1}{F_1/\sigma_{\omega,1} + (1-F_1)/\sigma_{\omega,2}} \end{cases} \tag{6}$$

$$\begin{cases} F_1 = \tanh\left(\left(\min\left[\max\left(\dfrac{\sqrt{k}}{0.09\omega Y}, \dfrac{500\mu}{\rho Y^2 \omega}\right), \dfrac{4\rho k}{\sigma_{\omega,2} D_{\omega}^{+} Y^2}\right]\right)^4\right) \\ F_2 = \tanh\left(\left[\max\left(2\dfrac{\sqrt{k}}{\beta^* \omega Y}, \dfrac{500\mu}{\rho Y^2 \omega}\right)\right]^2\right) \\ D_{\omega}^{+} = \max\left[2\rho \dfrac{1}{\sigma_{\omega,2}} \dfrac{1}{\omega} \dfrac{\partial k}{\partial x_{\mathrm{j}}} \dfrac{\partial \omega}{\partial x_{\mathrm{j}}}, 10^{-10}\right] \end{cases} \tag{7}$$

$$\begin{cases} \alpha = F_1 \alpha_1 + (1-F_1)\alpha_2 \\ \beta = F_1 \beta_1 + (1-F_1)\beta_2 \end{cases} \tag{8}$$

In the calculation process, the following values are used: β^* = 0.09, α_1 = 0.556, β_1 = 0.075, $\sigma_{\mathrm{k,l}}$ = 0.85, $\sigma_{\omega,1}$ = 0.5, α_2 = 0.44, β_2 = 0.0828, $\sigma_{\mathrm{k},2}$ = 1, and $\sigma_{\omega,2}$ = 0.856.

The enthalpy-porosity Method is employed to solve the melting process of the PCM inside the spherical capsules. The present study adopts the following assumptions: (a) the liquid PCM is modeled as an incompressible Newtonian fluid; (b) its flow is laminar and transient; (c) density is treated as constant except in the buoyancy term, where the Boussinesq approximation applies; and (d) viscous dissipation and solid PCM displacement/settling are neglected. The governing equations used in this study are based on previous research (Jia et al., 2024b). The initial temperature of the packed channel is set to 300 K, with the inlet air temperature fixed at 333 K. The inlet *Re* for all packed channels is maintained at 3,000, and the outlet is defined as a pressure outlet condition. The PISO algorithm is employed to solve the momentum transport equations to derive the velocity and the pressure field. Both the momentum and thermal energy equations are processed using the second-order upwind scheme, and the pressure field is processed using the PRESTO scheme. The time term discretized via a second-order implicit approach. The under-relaxation factors used in the present study are 1, 0.8, 0.8, 1, 0.6 and 0.9 for the density, body forces, turbulent kinetic energy, specific dissipation rate, turbulent viscosity, energy and liquid fraction, respectively. The convergence criteria for all governing equations is set as 10^{-5}.

3.2 Model validation

To address the issue of grid contact points, a reduced sphere diameter model is employed, scaling the diameter of the spherical capsules to 99 % of their original value. The computational domain is discretized using polyhedral meshes, with boundary layers applied at the fluid-wall interfaces. The maximum grid size in the mainstream area remains at 1/30 D. When the maximum grid size in the capsule area is 1/120 D and 1/150 D, the deviation of the complete melting time is 0.43 %, achieving a grid-independent solution. A physical model consistent with that in the study by Athawale et al. (2022) is established, and the same parameter are applied. The temporal evolution of the liquid fraction obtained from the numerical solution is compared with their results, revealing a deviation within 10 %. This confirms the accuracy of the numerical model constructed in this study.

4. Results and discussion

The spherical capsules along the main flow direction are numbered sequentially from 1~8. Since the capsules near the inlet and outlet sections are inevitably affected by inlet and outlet effects, the analysis focused on the intermediate capsules (i.e., capsules 3 to 6) to accurately compare the influence of the channel-to-particle diameter ratio. Figure 3 illustrates the temporal evolution of the liquid fraction during the melting process of the PCM in capsules 3 to 6 for four different channel-to-particle diameter ratios. As time progresses, the melting rate of the PCM inside the spherical capsules gradually slows down, which is attributed to the increased thermal resistance between the melted liquid PCM and the capsule walls. Along the main flow direction, the melting rate of the PCM in the spherical capsules decreases, but the extent of this reduction varies with different channel-to-particle diameter ratios. At *N* = 1.3 and 1.47, the temporal evolution of the liquid fraction in capsules 3 to 6 nearly overlaps, indicating that increasing the channel-to-particle diameter ratio enhances the synchronization of the PCM melting process in spherical capsules at different locations.

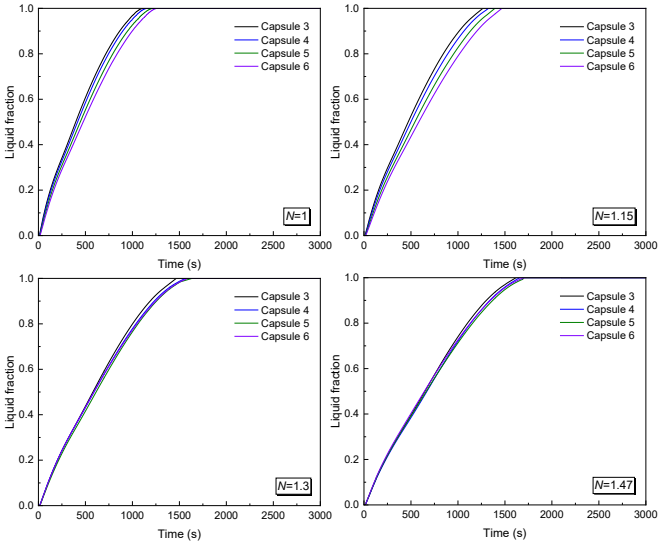

Figure 3: Temporal evolution of the liquid fraction at different channel-to-particle diameter ratios

Figure 4 illustrates the time required for the PCM inside spherical capsules at different positions to achieve complete melting under various *N*. It can be observed that for spherical capsules with the same sequence number, the time required for complete melting increases with *N*. Compared to the channel with *N* = 1, the complete melting time of PCM at different positions increases by an average of 14.32 %, 31.26 %, and 28.7 % for *N* = 1.15, 1.3, and 1.47, respectively. This indicates that the case with *N* = 1 exhibits the fastest melting rate. This phenomenon may be related to the inlet velocity: in this study, although the *Re* remains constant, the inlet velocity decreases as N increases due to differences in the hydraulic diameter and porosity of the packed channels. This reduction in inlet velocity weakens the convective heat transfer process between the heat transfer fluid and the spherical capsules, thereby affecting the melting process of the PCM inside the capsules.

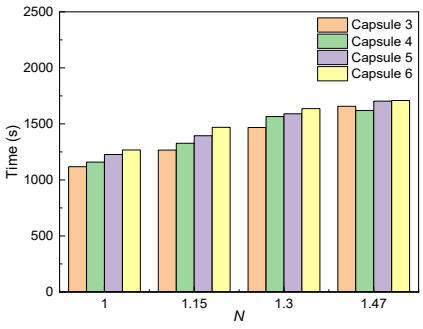

Figure 4: Complete melting time of PCM at different channel-to-particle diameter ratios

5. Conclusions

In this study, the convective heat transfer process between the heat transfer fluid and the spherical capsules, the phase change process of the PCM inside the spherical capsules, and the natural convection of the liquid PCM are simultaneously considered. Based on the SST *k-ω* equations and the enthalpy-porosity method, the influence of different channel-to-particle diameter ratios on the melting process of PCM in the packed channel is numerically investigated. Through a comparative analysis of the liquid fraction and complete melting time in spherical capsules at different *N* values and positions, the results demonstrate that the *N* has a significant impact on the thermal storage and melting process of PCM inside the spherical capsules. Under the same *Re* condition, increasing *N* reduces the melting rate of PCM while enhancing the synchronization of the melting process in spherical capsules at different positions.

Acknowledgments

The work is financially supported by National Natural Science Foundation of China (No. 52076169).

References

Alva G., Liu L., Huang X., Fang G., 2017, Thermal energy storage materials and systems for solar energy applications. Renewable and Sustainable Energy Reviews, 68, 693–706.

Athawale V., Jakhar A., Jegatheesan M., Rath P., Bhattacharya., 2022, A 3D resolved-geometry model for unstructured and structured packed bed encapsulated phase change material system. Journal of Energy Storage, 51, 104430.

Cheng X., Zhai X., 2017, Thermal performance analysis of a novel PCM capsule in red blood cell shape. Applied Thermal Engineering, 120, 130–137.

Dong Y., Wang F., Zhang Y., Shi X., Zhang A., Shuai Y., 2022, Experimental and numerical study on flow characteristic and thermal performance of macro-capsules phase change material with biomimetic oval structure. Energy, 238, 121830.

Ghojavand F., Baniasadi E., Afshari E., Genceli H., 2023, Simulation and performance analysis of a cooling energy storage system based on encapsulated nano-enhanced phase change materials. Energy Storage, 5, e424.

Guo W., He Z., Mawire A., Zhang P., 2023, Parametric investigation of charging and discharging performances of a cascaded packed bed thermal energy storage system. Journal of Energy Storage, 57, 106229.

He X., Qiu J., Wang W., Hou Y., Ayyub M., Shuai Y., 2023, Optimization design and performance investigation on the cascaded packed-bed thermal energy storage system with spherical capsules. Applied Thermal Engineering, 225, 120241.

He X., Oiu J., Wang W., Hou Y., Ayyub M., Shuai Y., 2022, A review on numerical simulation, optimization design and applications of packed-bed latent thermal energy storage system with spherical capsules. Journal of Energy Storage, 51, 104555.

Hu G., Zhang H., Liu Q., 2022, Design optimization on characteristics of packed-bed thermal energy storage system coupled with high temperature gas-cooled reactor pebble-bed module. Energy Conversion and Management, 257, 115434.

Hu Z., Xue D., Wang W., Tian H., Yin Q., Xuan Y., Chen D., 2023, Numerical investigation of the melting characteristics of spherical-encapsulated phase change materials with composite metal fins. Journal of Energy Storage, 68, 107902.

Jia H., Yang J., Wang T., Tian Y., Wang Q., 2024a, Numerical simulation on the impact of dimpled structure on flow and thermal performance in phase-change spherical capsules within confined spaces. Journal of Energy Storage, 99, 113213.

Jia H., Yang J., Zhou Z., Tian Y., Wang Q., 2024b, Numerical and three-factor design investigation for melting process of phase-change spherical capsules in a solar thermal energy storage system. Journal of Energy Storage, 85, 111094.

Li J., Wang W., Deng Y., Gao L., Bai J., Xu L., Chen J., Yuan Z., 2023, Thermal performance analysis of composite phase change material of myristic acid-expanded graphite in spherical thermal energy storage unit. Energies, 16, 4527.

Mao Q., Cao W., 2023, Study on the thermal storage performance of high-temperature molten salt spheres packed bed using different heat transfer fluids. Journal of Energy Storage, 66, 107420.

Mao Q., Zhang Y., 2020, Thermal energy storage performance of a three-PCM cascade tank in a high-temperature packed bed system. Renewable Energy, 152, 110–119.

Sharma A., Kothari R., Sahu S.K., 2022, Effect of fin location on constrained melting heat transfer of phase change material in a spherical capsule: A numerical study. Journal of Energy Storage, 52, 104922.

Wang J., Yang J., Cheng Z., Liu Y., Chen Y., Wang Q., 2018, Experimental and numerical study on pressure drop and heat transfer performance of grille-sphere composite structured packed bed. Applied Energy, 227, 719-730.

Wang W., He X., Shuai Y., Qiu J., Hou Y., Pan Q., 2022, Experimental study on thermal performance of a novel medium-high temperature packed-bed latent heat storage system containing binary nitrate. Applied Energy, 309, 118433.

Wang F., Zhang G., Shi X., Dong Y., Xun Y., Zhang A., 2022, Biomimetically calabash-inspired phase change material capsule: Experimental and numerical analysis on thermal performance and flow characteristics. Journal of Energy Storage, 52, 104859.

Yu C., Qian J., Cao D., Chen D., Wu L., Zhang C., 2023, Charging performance of structured packed-bed latent thermal energy storage unit with phase change material capsules. Journal of Energy Storage, 71, 108157.